

2D numerical simulation of lunar response to gravitational waves using finite element method

Lei Zhang^{1,*}, Han Yan^{2,3,*}, Xian Chen^{2,3,†} and Jinhai Zhang^{1‡}

¹*Research Center for Deep Earth Technology and Equipment,*

*State Key Laboratory of Deep Petroleum Intelligent Exploration and Development,
Institute of Geology and Geophysics, Chinese Academy of Sciences, Beijing 100029, China*

²*Department of Astronomy, School of Physics, Peking University, 100871 Beijing, China and*

³*Kavli Institute for Astronomy and Astrophysics at Peking University, 100871 Beijing, China*

(Dated: December 25, 2024)

Previous studies of the response of the Moon to gravitational waves have been carried out using analytical or semi-analytical models assuming ideal lunar structures. Such models are advantageous for their high-speed calculation but fail to account for the extremely heterogeneous subsurface and/or interior structures of the Moon. Numerical calculations are needed, but it is challenging to model the topography and lateral heterogeneity of the Moon. In addition, the computational cost is great especially when performing the GW simulation for a long time. As a first step towards overcoming the above difficulties, we employ a two-dimensional finite element method to numerically simulate the lunar response to gravitational waves. We verify our method by comparing our numerical results with those semi-analytical solutions. Based on such comparison, we also analyze the limitation of the two-dimensional simulation. Our work breaks a new way towards the precise simulation of realistic lunar response to gravitational waves in the future and lays down a solid foundation for three-dimensional numerical simulations.

I. INTRODUCTION

The search for gravitational wave (GW) in both $10 - 10^2$ Hz [1] range as well as nano-Hz [2–5] range has achieved great success, which strongly motivates the search in other frequency bands. For example, several space-based interferometers have been proposed to detect milli-Hertz (mHz) GWs, including the Laser Interferometer Space Antenna (LISA [6]), TianQin [7], and Taiji [8]. For the deci-Hertz (0.1 Hz, or deci-Hz) band, one possibility which has been considered for a long time is to use Earth or the Moon as a resonator to detect GWs [9–11]. In this direction, there is increasing interest recently to use an array of lunar seismometers to increase the sensitivity to GW, such as the proposed Lunar GW Antenna (LGWA) [12–14] and other similar proposals [15].

Several recent works carefully looked into the response functions of the Moon to GWs [16–19]. They resolved the apparent discrepancy between the results derived using different forms of the GW force density, and provided a consistent understanding of how to apply the response functions. However, these works also showed that the result is sensitive to (i) the details in the lunar structure, such as the fine structure near the surface or the parameters of different lays [12, 15, 19, 20], as well as (ii) the details in the numerical calculation of the normal modes, e.g., assuming spherical Moon or infinite half plane, using MINEOS or other eigen-mode solvers [20, 21]. To help us better decide the instrument sensitivity and select landing site for lunar seismic GW detector, a global

response function accounting for realistic lunar structure is still essential.

As we know, the Moon had experienced long-term and heavy bombardments in history, which resulted in a great number of fractures and holes in the lunar crust [22–27]. These fine structures could distort the path of seismic wave propagation [27]. Besides, the topography of the Moon is fairly rough, due to the impacts and volcano activities [28, 29]. However, previous theoretical approaches or semi-analytical methods have difficulty in resolving the topography and lateral heterogeneity of the Moon. Consequently, it is necessary to employ purely numerical simulation techniques to establish a nonuniform lunar model and calculate its response to GW. Among the various numerical simulation methods available, the finite element method (FEM) is widely utilized due to its flexibility in handling geometric shapes [30], coupling of multiple physical fields[31], and well-developed parallel computing [32]. Therefore, this study adopts the spectral element method (SEM) [33]—a high-order FEM—to model the entire Moon and calculate its seismic response to GWs.

The paper is organized as follows. In Section II we revisit the theory of calculating the lunar response functions, and provide an updated formula in the frequency domain. In Section III, we illustrate the settings and related details in our FEM simulation. In Section IV, we present our new results from FEM calculation, focusing on the angular dependency as well as the radial and horizontal response functions. In Section V, we discuss the effects which can affect the accuracy of our simulation, including the angular resolution and the 2D nature of our model. In Section VI, we draw a conclusion to this work, and point out several caveats to be investigated in the future. Throughout the paper we adopt the International

* The first two authors contributed equally to this work.

† xian.chen@pku.edu.cn

‡ zjh@mail.iggcas.ac.cn

System of Units, unless mentioned otherwise.

II. REVIEW OF THE THEORY OF LUNAR RESPONSE TO GW

In this section, we first review the basic formulation of the lunar response to GWs. We only modify the part related to the source-time function (STF), which allows us to derive the response function for a wide range of frequencies at once, in a single simulation.

As it has been studied in many previous works [16, 17, 34], given a linearly polarized GW propagating along z -axis with an amplitude h_0 and a STF $g(t)$,

$$\begin{aligned} \mathbf{h} &= h_0 \epsilon_{ij} g(t), \\ \epsilon_{ij} &= \begin{bmatrix} 1 & 1 & 0 \\ 1 & -1 & 0 \\ 0 & 0 & 0 \end{bmatrix}, \end{aligned} \quad (1)$$

the surface response of a radially heterogeneous elastic sphere can be written as:

$$\vec{\xi}(\theta, \varphi, t) = h_0 \sum_n \sum_{m=-2}^2 \vec{s}_{nm}(\theta, \varphi) \Re\{\bar{g}_n(t)\} f^m \alpha_{2n}, \quad (2)$$

where (θ, φ) follow the standard definition in a spherical coordinate, and the corresponding location in (x, y, z) coordinate at the surface is $R(\sin\theta \cos\varphi, \sin\theta \sin\varphi, \cos\theta)$ (R is the lunar radius). \vec{s}_{nm} is the displacement eigenfunction, f^m is the ‘‘pattern function’’ related to GW wave vector and polarization, α_{2n} is the part depending on the radial structure, and $\bar{g}_n(t)$ is the time-dependent part we will discuss below.

According to previous analyses [16, 19, 34], in the limit of $Q_n \gg 1$, the time-dependent part $\bar{g}_n(t)$, can be calculated as:

$$\bar{g}_n(t) = \frac{1}{2\pi} \int d\omega e^{i\omega t} \frac{1 + \frac{i\omega}{2Q_n\omega_n}}{\omega_n^2 - \omega^2 + i\omega_n\omega/Q_n} g(\omega), \quad (3)$$

where $g(\omega) = \int dt e^{i\omega t} g(t)$ is the Fourier transform of the STF. Thus following the definitions in [17, 19], the lunar response per unit strain can then be written in a more concise form in the frequency domain:

$$\begin{aligned} \vec{\xi}(\theta, \varphi, f)/h_0 &= \mathcal{F}\{\vec{\xi}(\theta, \varphi, t)\}/h_0 \\ &= g(\omega) \times \\ &\left[T_r(\omega) \sum_m f^m \mathcal{Y}_{2m}(\theta, \varphi) \hat{e}_r \right. \\ &+ T_h(\omega) \sum_m f^m \partial_\theta \mathcal{Y}_{2m}(\theta, \varphi) \hat{e}_\theta \\ &\left. + T_h(\omega) \sum_m f^m \frac{\partial_\varphi \mathcal{Y}_{2m}(\theta, \varphi)}{\sin\theta} \hat{e}_\varphi \right], \end{aligned} \quad (4)$$

in which $\omega = 2\pi f$, and the radial and horizontal response functions in the frequency domain are defined as

$$\begin{aligned} T_r(\omega) &\equiv \sum_n U_{2n} \alpha_{2n} \Re\left\{ \frac{1 + \frac{i\omega}{2Q_n\omega_n}}{\omega_n^2 - \omega^2 + i\omega_n\omega/Q_n} \right\} \\ T_h(\omega) &\equiv \sum_n \frac{V_{2n}}{\sqrt{6}} \alpha_{2n} \Re\left\{ \frac{1 + \frac{i\omega}{2Q_n\omega_n}}{\omega_n^2 - \omega^2 + i\omega_n\omega/Q_n} \right\}. \end{aligned} \quad (5)$$

The details of \vec{s}_{nm} , f^m , α_{2n} , U_{2n} , V_{2n} and \mathcal{Y}_{2m} can all be found in [17] and other related works.

In the numerical simulations of this work, we only consider the response on the $x - y$ plane (i.e., $\theta = \pi/2$). In this case, Eq. (4) can be further simplified as

$$\begin{aligned} \vec{\xi}(\varphi, f)/h_0 &= g(\omega) \times \\ &\left[T_r(\omega) (\sin 2\varphi + \cos 2\varphi) \hat{e}_r \right. \\ &\left. + 2T_h(\omega) (-\sin 2\varphi + \cos 2\varphi) \hat{e}_\varphi \right]. \end{aligned} \quad (6)$$

III. FINITE ELEMENT SIMULATION

Although theoretical or semi-analytical solutions can provide the response of lunar GW, they do not account for the rough topography (e.g., impact craters or volcanos) or the fluctuant subsurface structures (e.g., local geological body and asymmetric lunar core). Therefore, there is an urgent need to develop a practicable scheme of numerically simulating the lunar response to GWs. In this section, we describe our scheme of 2D FEM simulation and the corresponding parameter configurations.

The SEM has been widely used in the field of seismic wave simulations in the past decades ([35]) due to its high precision and great feasibility in high performance parallel computing ([33]). Herein we extend the 2D SEM to study the impact of GW on the Moon. Our simulation is based on SPECSEM2D ([36, 37]), and we implement the forces induced by GWs in the program and conduct a long-time simulation. A global 2D lunar model composed of 140,576 fourth-order spectral elements has been built up (Fig. 1a), based on the same model as in Ref. [17] with coarser layering near the surface. The original model file *Model_FEM.txt* can be found in [38]. The grid size is approximately 3.7 km in the horizontal direction on the ground surface, and it increases according to the seismic wave velocities to avoid the artifacts caused by numerical dispersion that is associated with using course grid, as shown in Fig. 1b. The highest frequency that can be accurately resolved by the model is approximately 0.2 Hz. The maximum allowed time step is approximately 0.035 s from the perspective of numerical stability.

Based on our previous work [17], we decide to choose a Dyson-type force density [39],

$$\vec{f} = \nabla\mu \cdot \mathbf{h}, \quad (7)$$

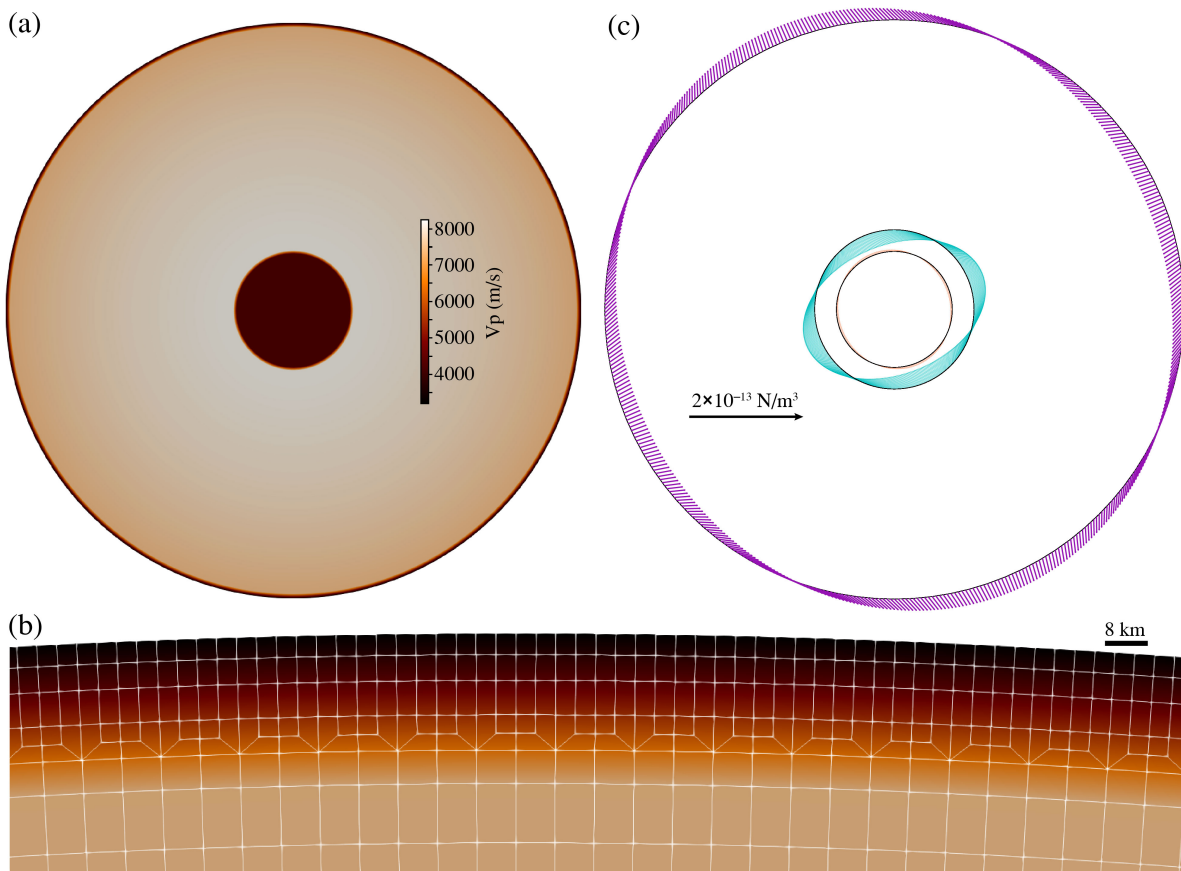


FIG. 1. The SEM model for our simulation. (a) Layered global model of the entire Moon. The color represents the value of the P-wave velocity; (b) Enlarged regional crust grids near the azimuth of 0° , with a surface element size of about 3.7 km. (c) The distribution of the force density vector with an azimuthal resolution of 1° . The black arrow shows a scale of $2 \times 10^{-13} \text{ N/m}^2$ for reference.

to calculate the lunar response to GWs, where \mathbf{h} has the same form as in Eq. (1). This kind of force density is mainly located in the layers with large radial variation of shear modulus $\mu (= \rho v_s^2)$, so it should be varied correspondingly when the lunar model (thereby, grids) near these layers changes, in order to maintain the total value of the force. The distribution of the force density is shown in Fig. 1c, where we have assumed $h_0 = 10^{-20}$. Here we add force vectors directly. The magnitude of the force equals force density times the volume involved, where the involved volume should be calculated by the force-covering area times 1 m, the thickness of our 2-D Moon model [40]. The spatial resolution in the tangential direction (azimuth resolution) is 1.00° (Fig. 1c). As a result, 4320 individual forces have been applied in the entire Moon.

Each force can be regarded as an individual point force. For the purpose of our numerical simulations, the ideal STF should result in a perturbation of the Moon across a wide frequency band since we focus on a wide frequency range of GW (1~20 mHz). Herein we use the STF of Gaussian wavelet with a dominant frequency of 20 mHz.

The entire simulation duration is up to 100,000 s, which allows seismic waves to propagate inside the Moon for tens of rounds. The spectrum of the STF is presented in Fig. 2. We can see that the normalized amplitude is flat in the frequency range < 20 mHz. The simulation was completed on the National Supercomputing Center in Wuxi, China. An individual node of the cluster has a total memory of 512 GB and consists of 64 cores, which means that up to 64 processes can simultaneously share the memory. Since we conducted a long-time simulation to study the response of the Moon over a period of 100,000 s, large amount of memory is always required even for a 2D case. Therefore, we restrict the number of processes on each node to 10 to ensure that each process has sufficient memory. As a result, the wall-clock time consumption is about 0.5 hours using 192 nodes with 12,288 cores.

Based on the FEM model (Fig. 1), the lunar seismic response to GW has been simulated. From the radial acceleration snapshots (Fig. 3), we find that the motion originates at the same location where we add the force (Fig. 3a). The response generated at the core-mantle

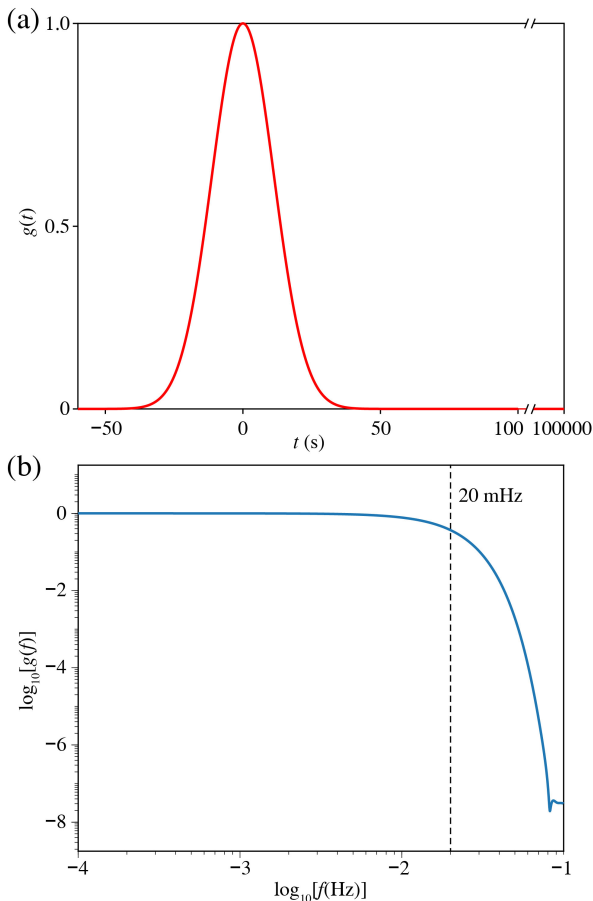


FIG. 2. Source time function (dimensionless) with a dominated frequency of 20 mHz. The result is normalized to have a maximum value of 1. (a) The STF $g(t)$ for a duration of 100,000 s. (b) The normalized amplitude spectral distribution $g(f)$.

boundary propagates outward, and meets the response generated at the lunar crust (Figs. 3abc). The seismic waves interact with each other after meeting, and then spread throughout the Moon (Fig. 3def), leading to a global oscillation of the Moon. During this process, normal modes of the Moon are excited and can be recorded on the surface of the Moon. Fig. 4 shows more snapshots of the radial velocity.

IV. NUMERICAL RESULTS OF LUNAR SURFACE RESPONSE

In this section, we will analyze the main results from our FEM simulations. We first analyze the angular dependency of the lunar response at different frequencies. We perform Fourier transform of the lunar surface displacement, and obtain the values of $|\xi_r(\varphi, f)|$ and $|\xi_h(\varphi, f)|$ for different φ . To better compare with theory, we then select several typical frequencies, $f = 0.9$ mHz, 1.68 mHz and 2.8 mHz, and fit the amplitude of the lunar

surface oscillation assuming an angular dependence given by Eq. (6). These three selected frequencies correspond to the first three resonant peaks from FEM simulation (see Fig. 6), where the response reaches local maximum in the frequency domain. The results are plotted in Fig. 5. We find that the numerical results match generally well with the theoretical relation in Eq. (6), but we also see a slight deviation for the horizontal response.

Next, we want to directly obtain $T_r(f)$ and $T_h(f)$ from our numerical results. Our approach is to first calculate $|\xi_r(f, \varphi)/h_0 g(\omega)|$ and $|\xi_h(f, \varphi)/h_0 g(\omega)|$ for each output position. We eliminate the angular variation by averaging over φ and then modifying it by a factor of $2\sqrt{2}/\pi \simeq 0.9$, which comes from the average of $|\sin 2\varphi \pm \cos 2\varphi|$ [notice another factor of 2 for the horizontal response, see Eq. (6)]. The results are plotted in Fig. 6. In our calculation we set $h_0 = 10^{-20}$, which explains the different amplitudes with respect to Fig. 5. We will compare this result with the previous semi-analytical prediction (from Sec. II) in Sec. V.

V. DISCUSSIONS

Since we use FEM to discretize the entire Moon, the locations where we add the forces depend on our choice of the resolution. Such spatial resolution of force density (angular resolution), in principle, should not affect the simulation results if the resolution is sufficiently high. For this reason, we have tested the effects of different angular resolutions ($\Delta\varphi = 0.75^\circ, 1.00^\circ, 1.25^\circ$) on waveform and ground amplitude (Fig. 7). The difference in amplitude among the three is less than 0.1%. Therefore, we have chosen $\Delta\varphi = 1.00^\circ$ as our fiducial resolution. In addition, we would like to emphasize that the Dyson-type force density (Eq. 7) is added at the interface where the shear modulus and S-wave velocity vary drastically. The way of constructing the grids and adding the force at these places could affect the numerical results of the lunar response to GWs, which is worth investigating in the future.

To compare the results from our FEM calculation and those from previous semi-analytical approaches (in Sec. II), we plot these two kinds of response functions in Fig. 8. The gray lines are response functions calculated with the approach described in Sec. II, using the same lunar model as in the FEM calculation. The blue lines are the same response functions as in Fig. 6, but horizontally translated by about 0.06 dex to compensate for the difference between 2D (numerical) and 3D (analytical) models. We find that the two types of response functions match qualitatively well in the frequency range of 1~20 mHz, especially regarding the order of magnitude and the locations of the first few resonant peaks. Although we only simulate lunar response to GW in the frequency band of 1 mHz to 20 mHz, it does not mean that we are limited to this frequency band. In fact, we can handle higher frequency band (e.g., up to 200 mHz based on the

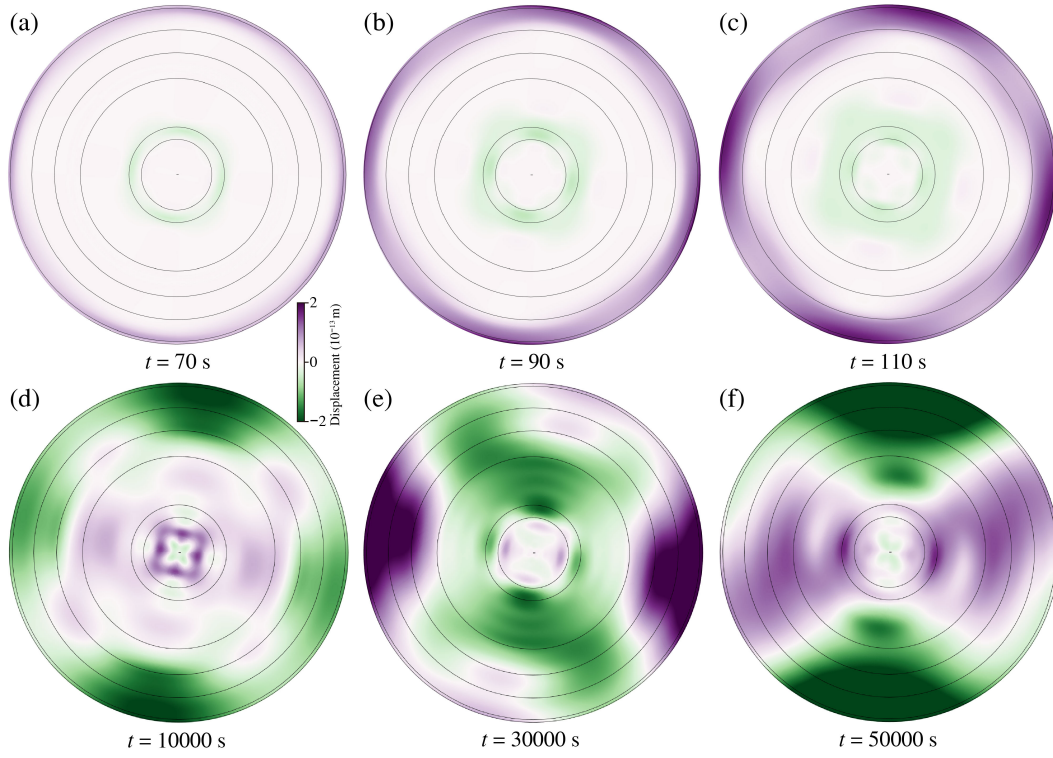


FIG. 3. Representative snapshots of the radial displacement of the Moon driven by passing GWs. See the radial displacement movie *Dis_snapshots.gif* in [38]. (a) $t = 70$ s; (b) $t = 90$ s; (c) $t = 110$ s; (d) $t = 10,000$ s; (e) $t = 30,000$ s; (f) $t = 50,000$ s.

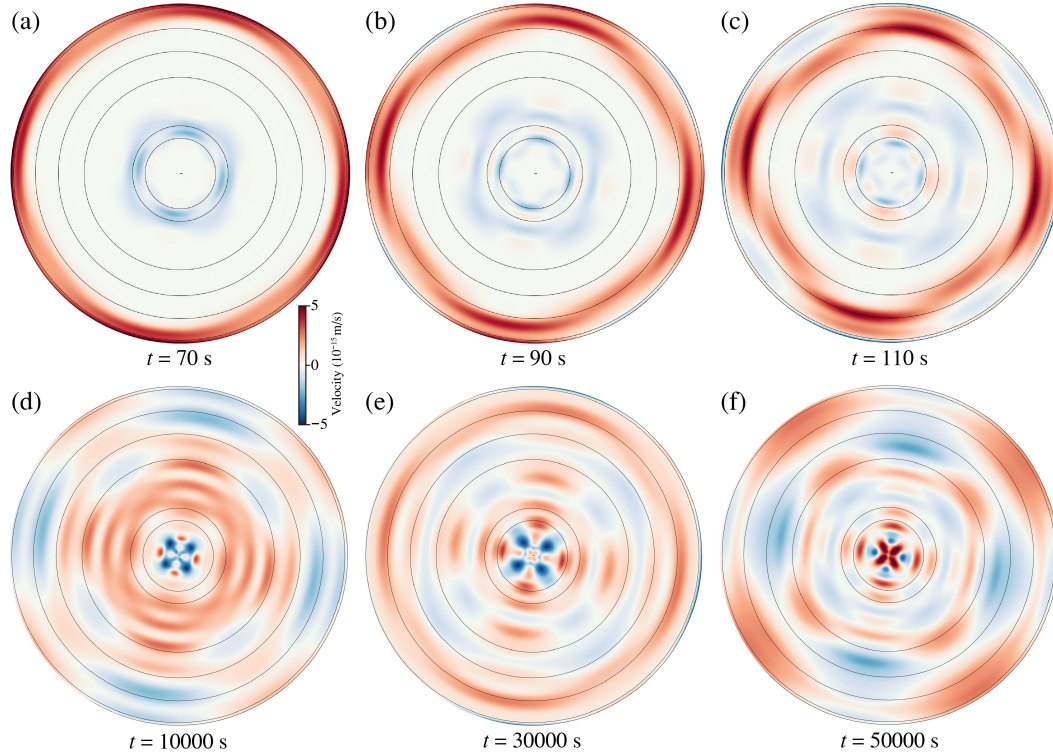


FIG. 4. Representative snapshots for the radial velocity. (a) $t = 70$ s; (b) $t = 90$ s; (c) $t = 110$ s; (d) $t = 10,000$ s; (e) $t = 30,000$ s; (f) $t = 50,000$ s.

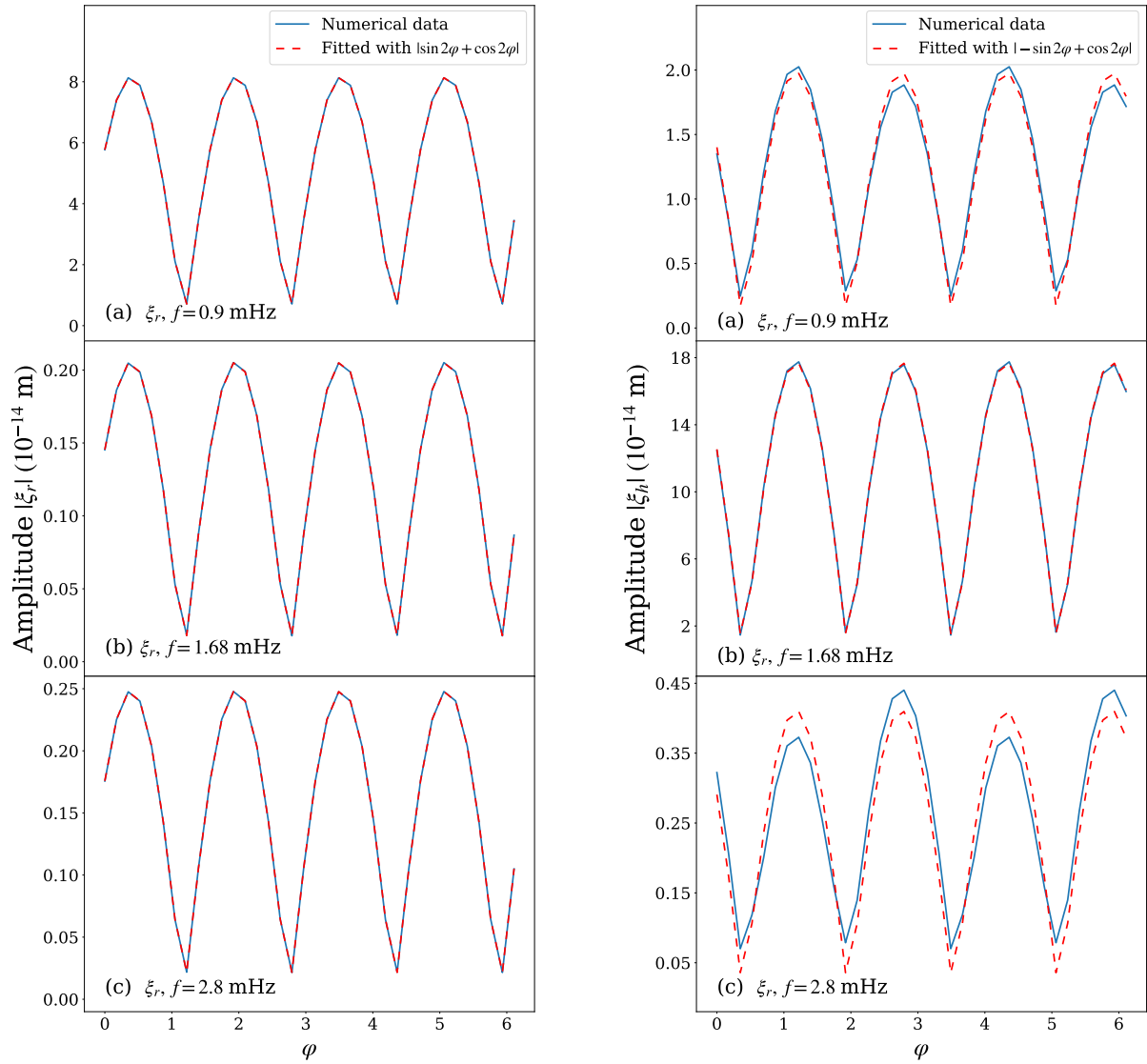


FIG. 5. Angular dependence of the radial response $|\xi_r(\varphi, f)|$ and horizontal response $|\xi_h(\varphi, f)|$. The red-dashed curves are fitting results using Eq. (6). (a)~(c) are radial results, (d)~(f) are horizontal results. The three selected frequencies $f = 0.9, 1.68$ and 2.8 mHz correspond to the first three resonant peaks.

model in this paper). Here for a highly robust and stable simulation, we have only used STF within 20 mHz (Fig. 2). With more computer clusters with larger memory in the future, we can handle a higher frequency band, such as up to 1 Hz.

Nevertheless, in Fig. 8 we can still find visible deviations in both the locations of high-frequency resonant

peaks and the amplitudes at spectral troughs. There are several possible reasons that cause these deviations. The main one could be the difference between the 2D (cylindrical) Moon model in the FEM simulation and the 3D (spherical) Moon model in those previous semi-analytical calculations. We give a simple but instructive analysis in Appendix A, which shows that the difference between 2D

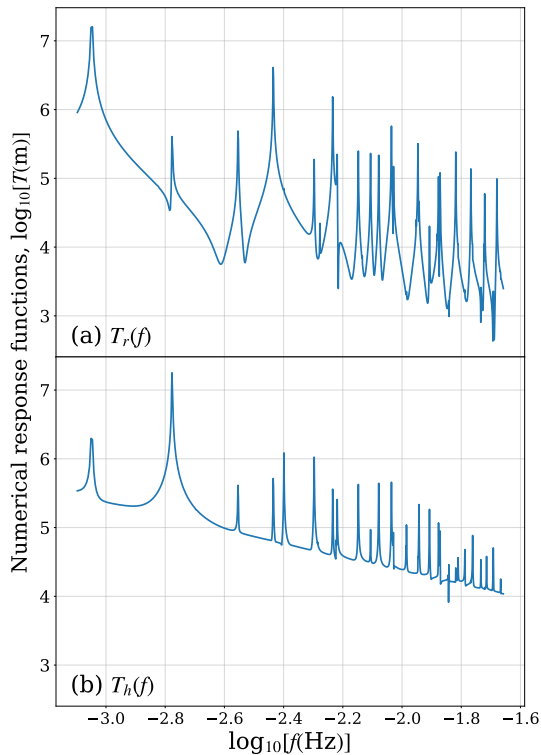


FIG. 6. Radial and horizontal response functions (log-scale) per unite strain from our FEM simulations. (a) Radial response function $T_r(f)$. (b) Horizontal response function $T_h(f)$.

and 3D models can lead to a shift of the first few eigenfrequencies around several mHz. The direction of the shift is determined by the details of the structure of the Moon, so that a numerical peak can reside at either the left- or the right-hand side of the analytical peak. The simple analysis explains our FEM results qualitatively, and it suggests that the different nature of the mathematical solutions in spherical and cylindrical coordinate, as well as the different types of the boundary conditions, can significantly change the eigen-frequencies and other related results. Since our 2D FEM predicts the locations and amplitudes of the strongest resonant peaks reasonably well, the method will be useful for the design of future seismic GW detection projects.

In the future, to realistically simulate the lunar response to GWs using FEM, a long period of simulation time is needed. Such a requirement poses a big challenge given the current memory size and computational resources. The problem will be even more severe when extending our model to 3D. Although we adopt a spherically symmetric uniform numerical model for the purpose of comparison with semi-analytical solutions, we have not

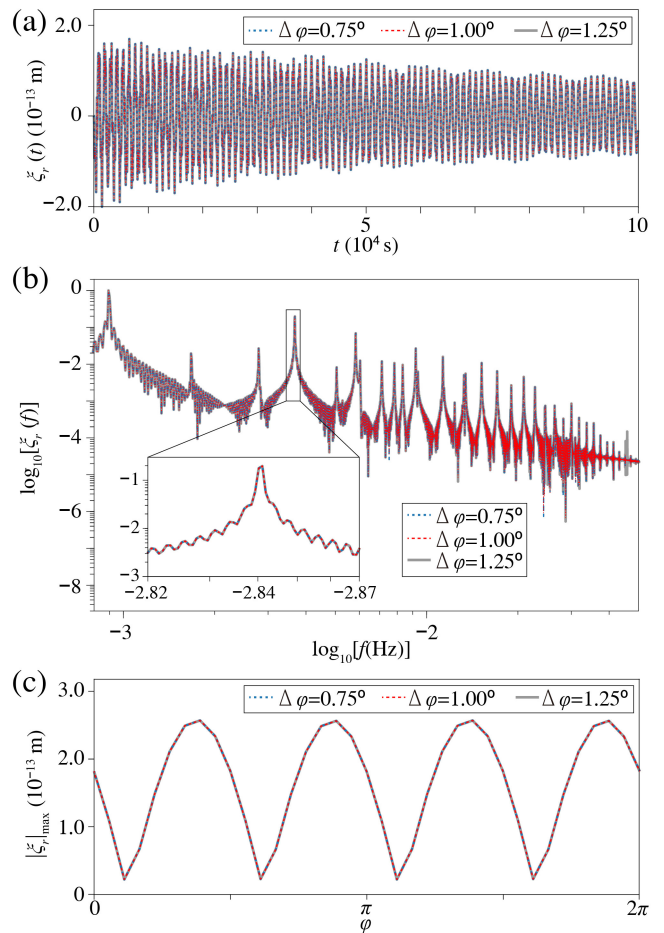


FIG. 7. Comparing the results derived from three different angular resolutions of the GW force density, namely, $\Delta\varphi = 0.75^\circ$, 1.00° , and 1.25° . (a) Waveform $\xi_r(t)$; (b) normalized spectrum $\xi_r(f)$ with the intersecting plot showing the details at the peak; (c) amplitude $|\xi_r|_{\max}$ of the waveform as a function of the azimuthal angle $\varphi = 0 \sim 2\pi$. Panels (a) and (b) are derived at $\varphi = 0^\circ$.

considered the actual conditions of the Moon such as topographic surface, fractured subsurface, or lateral variation of the interior structure. However, incorporating these aspects into FEM and/or SEM simulations, as well as extending them to 3D scenarios, poses no technical obstacles, and relevant technologies have just achieved breakthroughs[41]. Moreover, increasing the time step in FEM/SEM simulations is not straightforward due to the stability condition that must be satisfied (e.g., Courant-Friedrichs-Lewy condition). Therefore, the choice of time step is closely related to the spatial discretization and the wave propagation speed. In the future, to make 3D simulations feasible, it is crucial to implement specific schemes that allows larger time steps (e.g., see Refs. [42–44]).

ACKNOWLEDGMENTS

This work is supported by the National Natural Science Foundation of China (Grant Numbers: 42325406, 12473037, 42204178), Key Research Program of the CAS (Grant Numbers: ZDBS-SSW-TLC00104 and KGFZD-145-23-15-2) and Key Research Program of the Institute of Geology and Geophysics, Chinese Academy of Sciences (Grant Numbers: IGGCAS-202203 and IGGCAS-202102).

Appendix A: Compare the solutions in 3D (spherical) and 2D (cylindrical) models

In this appendix, we would like to give a semi-analytical explanation for the deviation between our numerical results and those previous theoretical ones. The deviation originates from the fact that in our FEM simulation, we use a 2D grid which represents an cylindrical “Moon” with infinite length. The radial distribution of this cylinder follows the same radial distribution of the 3D spherical Moon. To facilitate the comparison, we calculate the eigen-frequencies of two homogeneous “Moons”, one is spherical and the other is cylindrical. These two models have exactly the same physics parameters (radius R , density ρ , and two wave velocities v_p and v_s). The results can therefore be given analytically, as we will show below. Our calculation mainly follows Ref. [45], which originally is conducted for a sphere.

As has been proved previously, the spatial part of the eigen-vibrations $\mathbf{u}(\mathbf{x})$ with angular frequency $\omega (= 2\pi f)$ can be separated to an irrotational part and a divergence-free part:

$$\mathbf{u}(\mathbf{x}) = C_0 \nabla \phi(\mathbf{x}) + C_1 \mathbf{L}\psi(\mathbf{x}) + C_2 \nabla \times \mathbf{L}\psi(\mathbf{x}), \quad (\text{A1})$$

where C_0 , C_1 and C_2 are three constants, and $\mathbf{L} \equiv \mathbf{x} \times \nabla$. Therefore, the latter two terms are divergence-free.

The particular forms of $\phi(\mathbf{x})$ and $\psi(\mathbf{x})$ in cylindrical coordinates are different from those in spherical coordinates. In a spherical coordinate system (r, θ, φ) , as illustrated in Ref. [45], we have

$$\begin{aligned} \phi^S(\mathbf{x}) &= j_l(qr) Y_{lm}(\theta, \varphi), \\ \psi^S(\mathbf{x}) &= j_l(kr) Y_{lm}(\theta, \varphi), \end{aligned} \quad (\text{A2})$$

where j_l is l -th order spherical Bessel function, Y_{lm} is the spherical harmonic, and two wave numbers are defined as

$$\begin{aligned} q^2 &\equiv \frac{\rho}{\lambda + 2\mu} \omega^2, \\ k^2 &\equiv \frac{\rho}{\mu} \omega^2. \end{aligned} \quad (\text{A3})$$

In a cylindrical coordinate system (r, φ, z) , the corresponding forms are

$$\begin{aligned} \phi^C(\mathbf{x}) &= J_m(qr) e^{im\varphi}, \\ \psi^C(\mathbf{x}) &= J_m(kr) e^{im\varphi}, \end{aligned} \quad (\text{A4})$$

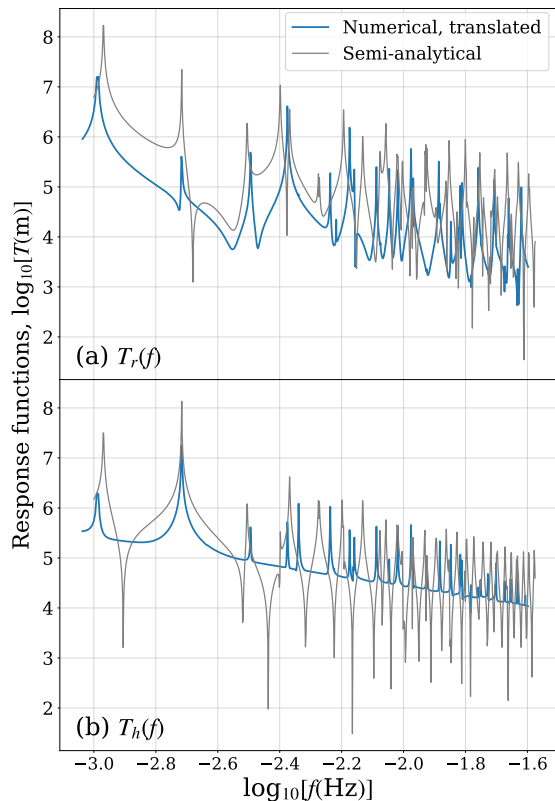


FIG. 8. Response function (log-scale) per unite strain from FEM simulation and previous semi-analytical approach. Numerical results have been horizontally translated. (a) Radial response function $T_r(f)$. (b) Horizontal response function $T_h(f)$.

VI. CONCLUSION

In this work, we conduct the first 2D FEM simulation of the lunar response to GWs. Compared to the previous semi-analytical models based on the normal-mode formalism, the FEM has great potential of accounting for the rough topography and the strong lateral heterogeneity of the lunar crust, and/or unique interior geometric structures. Our results suggest that in the ideal case of a symmetric Moon model, the response functions derived from FEM and previous semi-analytical approaches agree generally well, which means that our FEM simulation is feasible for calculating lunar response to GWs. In the future, FEM can further conduct 3D global Moon simulations, accounting for the topographic surface/fractured subsurface/lateral heterogeneous interior structure of the Moon.

where J_m is m -th order Bessel function.

To calculate the value of ω , we apply the free boundary condition $\sigma_{ij}n_j = 0$, in which $\sigma_{ij} \equiv \frac{1}{2}(u_{i,j} + u_{j,i})$ and n_j is the surface normal vector. For GWs, we only need to

consider the spheroidal mode [46], which means $C_1 = 0$. In spherical coordinate, the result has been derived in Ref. [45] which is

$$\det \begin{pmatrix} \beta_2^S(qR) - \frac{\lambda}{2\mu} q^2 R^2 \beta_0^S(qR) & l(l+1)\beta_1^S(kR) \\ \beta_1^S(qR) & \frac{1}{2}\beta_2^S(kR) + \left[\frac{l(l+1)}{2} - 1\right]\beta_0^S(kR) \end{pmatrix} = 0, \quad (\text{A5})$$

where

$$\beta_0^S(x) \equiv \frac{j_l(x)}{x^2}, \quad \beta_1^S(x) \equiv \frac{d}{dx} \left[\frac{j_l(x)}{x} \right], \quad \beta_2^S(x) \equiv \frac{d^2}{dx^2} [j_l(x)]. \quad (\text{A6})$$

In cylindrical coordinate, after some algebra, we find that

$$\det \begin{pmatrix} \beta_2^C(qR) - \frac{\lambda}{2\mu} \beta_0^C(qR) & \beta_2^C(kR) + m^2 \beta_1^C(kR) \\ 2\beta_1^C(qR) + \frac{\beta_0^C(qR)}{q^2 R^2} & \beta_2^C(kR) + 2\beta_1^C(kR) + \frac{m^2+1}{k^2 R^2} \beta_0^C(kR) \end{pmatrix} = 0, \quad (\text{A7})$$

where

$$\beta_0^C(x) \equiv J_m(x), \quad \beta_1^C(x) \equiv \frac{d}{dx} \left[\frac{J_m(x)}{x} \right], \quad \beta_2^C(x) \equiv \frac{d^2}{dx^2} [J_m(x)]. \quad (\text{A8})$$

For GWs, it is required that $l = 2$ in spherical coordinate. However, in cylindrical coordinate the choice of m is unclear so far (we will investigate this issue in the future), so we calculate both $m = 2$ and $m = 2.5$. The first one is the same as the l index in the spherical harmonic, and the second one comes from the mathematical relation between the Bessel function and the spherical Bessel function:

$$j_l(x) = \sqrt{\frac{\pi}{2x}} J_{l+0.5}(x), \quad l > 0.$$

We calculate the first few eigen-frequencies $f = \omega/2\pi$ for a homogeneous ‘‘Moon’’ with $R = 1737$ km, $\rho = 3 \times 10^3$ kg/m³, $v_p = 8 \times 10^3$ m/s and $v_s = 4 \times 10^3$ m/s [47–49] [notice that $\lambda = \rho(v_p^2 - 2v_s^2)$ and $\mu = \rho v_s^2$]. The results are listed in Table I. The frequencies in the $m = 2$ case are more similar to our numerical results. Since these frequencies are derived from a different lunar model (one is homogeneous and the other is heterogeneous), the comparison is not exact. We would also like to point out that, in principle, we can write down the complete

solutions based on Eq. (A1) and the particular form of the force density acting on the Moon. Nevertheless, the current comparison, also not exact, already qualitatively explains the deviation between our semi-analytical and numerical results.

TABLE I. First few eigen-frequencies for a 3D spherical ‘‘Moon’’ and a 2D cylindrical ‘‘Moon’’ with the same parameters.

	Mode	f (mHz)	Mode	f (mHz)	
Spherical	$l = 2$	0.971	Cylindrical	$m = 2$	0.666
		1.868			1.970
		3.161			3.087
		4.026			3.508
		4.505			4.300
	
			$m = 2.5$	0.917	
				2.217	
				3.330	
				3.966	
				4.575	
				...	

[1] B. P. Abbott, R. Abbott, T. D. Abbott, *et al.*, Observation of gravitational waves from a binary black hole merger, *Phys. Rev. Lett.* **116**, 061102 (2016), arXiv:1602.03837 [gr-qc].

[2] H. Xu, S. Chen, Y. Guo, *et al.*, Searching for the nano-

Hertz stochastic gravitational wave background with the Chinese Pulsar Timing Array Data Release I, *Research in Astronomy and Astrophysics* **23**, 075024 (2023), arXiv:2306.16216 [astro-ph.HE].

[3] EPTA Collaboration, InPTA Collaboration, *et al.*, The

- second data release from the European Pulsar Timing Array. III. Search for gravitational wave signals, *Astronomy & Astrophysics* **678**, A50 (2023), arXiv:2306.16214 [astro-ph.HE].
- [4] G. Agazie, M. F. Alam, A. Anumarlapudi, *et al.*, The NANOGrav 15 yr data set: Observations and timing of 68 millisecond pulsars, *The Astrophysical Journal Letters* **951**, L9 (2023), arXiv:2306.16217 [astro-ph.HE].
- [5] D. J. Reardon, A. Zic, R. M. Shannon, *et al.*, Search for an isotropic gravitational-wave background with the Parkes Pulsar Timing Array, *The Astrophysical Journal Letters* **951**, L6 (2023), arXiv:2306.16215 [astro-ph.HE].
- [6] P. Amaro-Seoane, H. Audley, S. Babak, *et al.*, Laser Interferometer Space Antenna, arXiv e-prints , arXiv:1702.00786 (2017), arXiv:1702.00786 [astro-ph.IM].
- [7] J. Luo, L. Chen, H. Duan, *et al.*, TianQin: a spaceborne gravitational wave detector, *Classical and Quantum Gravity* **33**, 035010 (2016), arXiv:1512.02076 [astro-ph.IM].
- [8] Z. Luo, Y. Wang, Y. Wu, W. Hu, and G. Jin, The Taiji program: A concise overview, *Progress of Theoretical and Experimental Physics* **2021**, 05A108 (2021).
- [9] J. Weber, Detection and Generation of Gravitational Waves, *Physical Review* **117**, 306 (1960).
- [10] J. Weber, Gravitational Waves, *Physics Today* **21**, 34 (1968).
- [11] T. S. Mast, J. E. Nelson, and J. A. Saarloos, Search for Gravitational Radiation from Pulsars, *Astrophysical Journal* **187**, L49 (1974).
- [12] J. Harms, F. Ambrosino, L. Angelini, *et al.*, Lunar Gravitational-wave Antenna, *Astrophys. J.* **910**, 1 (2021), arXiv:2010.13726 [gr-qc].
- [13] M. Branchesi, M. Falanga, J. Harms, *et al.*, Lunar Gravitational-Wave Detection, *Space Science Reviews* **219**, 67 (2023).
- [14] P. Ajith, P. Amaro Seoane, M. Arca Sedda, *et al.*, The Lunar Gravitational-wave Antenna: Mission Studies and Science Case, arXiv e-prints , arXiv:2404.09181 (2024), arXiv:2404.09181 [gr-qc].
- [15] J. Li, F. Liu, Y. Pan, Z. Wang, M. Cao, M. Wang, F. Zhang, J. Zhang, and Z. Zhu, Detecting gravitational wave with an interferometric seismometer array on lunar nearside, *Science China Physics, Mechanics, and Astronomy* **66**, 109513 (2023).
- [16] J. Majstorović, S. Rosat, and Y. Rogister, Earth's spheroidal motion induced by a gravitational wave in flat spacetime, *Phys. Rev. D* **100**, 044048 (2019).
- [17] H. Yan, X. Chen, J. Zhang, F. Zhang, M. Wang, and L. Shao, Toward a consistent calculation of the lunar response to gravitational waves, *Phys. Rev. D* **109**, 064092 (2024).
- [18] E. Belgacem, M. Maggiore, and T. Moreau, Coupling elastic media to gravitational waves: an effective field theory approach, *Journal of Cosmology and Astroparticle Physics* **2024** (7), 028, arXiv:2403.16550 [gr-qc].
- [19] J. Majstorović, L. Vidal, and P. Lognonné, Modeling lunar response to gravitational waves using normal-mode approach and tidal forcing, arXiv e-prints , arXiv:2411.09559 (2024), arXiv:2411.09559 [gr-qc].
- [20] X. Bi and J. Harms, Response of the Moon to gravitational waves, *Phys. Rev. D* **110**, 064025 (2024), arXiv:2403.05118 [gr-qc].
- [21] M. Kachelrieß and M. P. Nødtvedt, Lunar response to gravitational waves, *Phys. Rev. D* **110**, 064034 (2024), arXiv:2312.11665 [gr-qc].
- [22] P. Lognonné, J. Gagnepain-Beyneix, and H. Chenet, A new seismic model of the Moon: implications for structure, thermal evolution and formation of the Moon, *Earth and Planetary Science Letters* **211**, 27 (2003).
- [23] R. F. Garcia, J. Gagnepain-Beyneix, S. Chevrot, and P. Lognonné, Very preliminary reference Moon model, *Physics of the Earth and Planetary Interiors* **188**, 96 (2011).
- [24] R. C. Weber, P.-Y. Lin, E. J. Garnero, Q. Williams, and P. Lognonné, Seismic detection of the lunar core, *Science* **331**, 309 (2011).
- [25] C. Nunn, R. F. Garcia, Y. Nakamura, A. G. Marusiak, T. Kawamura, D. Sun, L. Margerin, R. Weber, M. Drilleau, M. A. Wiczorek, *et al.*, Lunar seismology: A data and instrumentation review, *Space Science Reviews* **216**, 89 (2020).
- [26] J. Zhang, B. Zhou, Y. Lin, M. H. Zhu, and Z. Ouyang, Lunar regolith and substructure at Chang'E-4 landing site in South Pole–Aitken basin, *Nature Astronomy* , 1 (2020).
- [27] X. Zhang, L. Zhang, J. Zhang, and R. N. Mitchell, Strong heterogeneity in shallow lunar subsurface detected by Apollo seismic data, *Journal of Geophysical Research: Planets* **127**, e2022JE007222 (2022).
- [28] B. Wang, Q. W. Zhang, Y. Chen, W. Zhao, Y. Liu, G. Tang, H. Ma, B. Su, H. Hui, J. W. Delano, *et al.*, Returned samples indicate volcanism on the Moon 120 million years ago, *Science* **385**, 1077 (2024).
- [29] Q. W. Zhang, M. Yang, Q. Li, Y. Liu, Z. Yue, Q. Zhou, L. Chen, H. Ma, S. Yang, X. Tang, *et al.*, Lunar farside volcanism 2.8 billion years ago from Chang'e-6 basalts, *Nature* , 1 (2024).
- [30] N. Moës, J. D. And, and T. Belytschko, A finite element method for crack growth without remeshing, *International Journal for Numerical Methods in Engineering* (1999).
- [31] L. Zhang, J. Zhang, R. N. Mitchell, P. Cao, and J. Liu, A thermal origin for super-high-frequency marsquakes, *Icarus* **390**, 115327 (2023).
- [32] G. Yagawa and R. Shioya, Parallel finite elements on a massively parallel computer with domain decomposition, *Computing Systems in Engineering* **4**, 495 (1993).
- [33] D. Komatitsch, S. Tsuboi, J. Tromp, A. Levander, and G. Nolet, The spectral-element method in seismology, *Geophysical Monograph-American Geophysical Union* **157**, 205 (2005).
- [34] A. Ben-Menahem, Excitation of the earth's eigenvibrations by gravitational radiation from astrophysical sources., *Nuovo Cimento C Geophysics Space Physics C* **6**, 49 (1983).
- [35] L. Zhang, J. Wang, Y. Xu, C. He, and C. Zhang, A procedure for 3D seismic simulation from rupture to structures by coupling SEM and FEM, *Bulletin of the Seismological Society of America* **110**, 1134 (2020).
- [36] D. Komatitsch and J.-P. Vilotte, The spectral element method: an efficient tool to simulate the seismic response of 2D and 3D geological structures, *Bulletin of the Seismological Society of America* **88**, 368 (1998).
- [37] D. Komatitsch and J. Tromp, Introduction to the spectral element method for three-dimensional seismic wave propagation, *Geophysical Journal International* **139**, 806 (1999).

- [38] <https://github.com/StrelitziaHY/LunarResponse>.
- [39] F. J. Dyson, Seismic Response of the Earth to a Gravitational Wave in the 1-Hz Band, *Astrophys. J.* **156**, 529 (1969).
- [40] L. Zhang, J. Zhang, and R. N. Mitchell, Dichotomy in crustal melting on early mars inferred from antipodal effect, *The Innovation* **3** (2022).
- [41] L. Zhang and J. Zhang, Local wavefield refinement using Fourier interpolation and boundary extrapolation for finite-element method based on domain reduction method, *Geophysics* **87**, T251 (2022).
- [42] Y. Gao, J. Zhang, and Z. Yao, Removing the stability limit of the explicit finite-difference scheme with eigenvalue perturbation, *Geophysics* **83**, A93 (2018).
- [43] Y. Gao, J. Zhang, and Z. Yao, Extending the stability limit of explicit scheme with spatial filtering for solving wave equations, *Journal of Computational Physics* **397**, 108853 (2019).
- [44] Z. Miao and J. Zhang, An optimal spatial-filtering method derived from eigenvalue perturbation for extending the Courant-Friedrichs-Lewy stability limit, *Geophysics* **88**, T227 (2023).
- [45] J. A. Lobo, What can we learn about gravitational wave physics with an elastic spherical antenna?, *Phys. Rev. D* **52**, 591 (1995), arXiv:gr-qc/0006102 [gr-qc].
- [46] M. Bianchi, E. Coccia, C. N. Colacino, V. Fafone, and F. Fucito, Testing theories of gravity with a spherical gravitational wave detector, *Classical and Quantum Gravity* **13**, 2865 (1996), arXiv:gr-qc/9604026 [gr-qc].
- [47] R. C. Weber, P. Lin, E. J. Garnero, Q. Williams, and P. Lognonné, Seismic Detection of the Lunar Core, *Science* **331**, 309 (2011).
- [48] R. F. Garcia, J. Gagnepain-Beyneix, S. Chevrot, and P. Lognonné, Very preliminary reference Moon model, *Physics of the Earth and Planetary Interiors* **188**, 96 (2011).
- [49] A. Briaud, C. Ganino, A. Fienga, A. Mémin, and N. Rambaux, The lunar solid inner core and the mantle overturn, *Nature* **617**, 743 (2023).